

Design of an array of folded patches

Blasi Luca¹, Mastrofini Alessandro², and Mucenica Stefan Leonard³

²email
³email

Abstract

Lorem ipsum dolor sit amet, consectetuer adipiscing elit. Ut purus elit, vestibulum ut, placerat ac, adipiscing vitae, felis. Curabitur dictum gravida mauris. Nam arcu libero, nonummy eget, consectetuer id, vulputate a, magna. Donec vehicula augue eu neque. Pellentesque habitant morbi tristique senectus et netus et malesuada fames ac turpis egestas. Mauris ut leo. Cras viverra metus rhoncus sem. Nulla et lectus vestibulum urna fringilla ultrices. Phasellus eu tellus sit amet tortor gravida placerat. Integer sapien est, iaculis in, pretium quis, viverra ac, nunc. Praesent eget sem vel leo ultrices bibendum. Aenean faucibus. Morbi dolor nulla, malesuada eu, pulvinar at, mollis ac, nulla. Curabitur auctor semper nulla. Donec varius orci eget risus. Duis nibh mi, congue eu, accumsan eleifend, sagittis quis, diam. Duis eget orci sit amet orci dignissim rutrum.

Nam dui ligula, fringilla a, euismod sodales, sollicitudin vel, wisi. Morbi auctor lorem non justo. Nam lacus libero, pretium at, lobortis vitae, ultricies et, tellus. Donec aliquet, tortor sed accumsan bibendum, erat ligula aliquet magna, vitae ornare odio metus a mi. Morbi ac orci et nisl hendrerit mollis. Suspendisse ut massa. Cras nec ante. Pellentesque a nulla. Cum sociis natoque penatibus et magnis dis parturient montes, nascetur ridiculus mus. Aliquam tincidunt urna. Nulla ullamcorper vestibulum turpis. Pellentesque cursus luctus mauris.

Introduction

Lorem ipsum dolor sit amet, consectetuer adipiscing elit. Ut purus elit, vestibulum ut, placerat ac, adipiscing vitae, felis. Curabitur dictum gravida mauris. Nam arcu libero, nonummy eget, consectetuer id, vulputate a, magna. Donec vehicula augue eu neque. Pellentesque habitant morbi tristique senectus et netus et malesuada fames ac turpis egestas. Mauris ut leo. Cras viverra metus rhoncus sem. Nulla et lectus vestibulum urna fringilla ultrices. Phasellus eu tellus sit amet tortor gravida placerat. Integer sapien est, iaculis in, pretium quis, viverra ac, nunc. Praesent eget sem vel leo ultrices bibendum. Aenean faucibus. Morbi dolor nulla, malesuada eu, pulvinar at, mollis ac, nulla. Curabitur auctor semper nulla. Donec varius orci eget risus. Duis nibh mi, congue eu, accumsan eleifend, sagittis quis, diam. Duis eget orci sit amet orci dignissim rutrum.

Tchebychev array factor design

A Tchebychev array factor will be designed in this part, so that the specific structure of the single element of the array is disregarded for the moment. The array is represented by a linear distribution of five elements ($n_{el} = 5$), which are supposed to be uniformly spaced and with a non-uniform amplitude for the feed arrangement, that anyway is going to be symmetrical (starting from the element in the middle, located in the origin of the geometrical axes). Also the "mean lobe to side lobe ratio" (R) will be one of the input design variables. Thus,

the variables of this design part are the *element inter-spacing* (d_{opt} , which needs to be optimal such that the beamwidth is minimized), the feed amplitude of the single antenna (each one represented by a C_i , with $i \in \{-2, -1, 0, 1, 2\}$, the i^{th} current coefficient - these unknowns are actually just three and not five, due to the symmetrical amplitude distribution hypothesis), the operating *resonant frequency* required for the single antenna (f) and some other quantities related to them, such as the *tapering efficiency* (η_T) and the *beamwidth* (BW_{fn}). Moreover, the difference between the beamwidth of the Tchebychev array (*Uniform Spacing Non Uniform Amplitude* case, shorten *NUA*) and that of a uniform array having the same number of elements and inter-spacing value but a uniform amplitude feed distribution (*Uniform Spacing Uniform Amplitude*, shorten *UA*) will be discussed. The input design variables related to the Tchebychev array factor (i.e. n_{el} , R and f) are listed in **table 1**.

Starting from the optimal inter-element spacing, it requires some secondary variables in orderer to be evaluated. Firstly, a coefficient (γ , depending on R and indirectly on the number of array elements) needs to be calculated, among with the wavelength in the free space (λ , as the ratio between the light speed in the free space - c - and the operating frequency f). Having those quantities, d_{opt} minimizing the BW_{fn} can be computed by using the **eq. (1)** group.

$$d_{opt} \rightsquigarrow \min\{BW_{fn}\}$$

$$d_{opt} = \lambda \left[1 - \frac{\arccos\left(\frac{1}{\gamma}\right)}{\pi} \right] \quad (1)$$

$$\gamma = \cosh \left[\frac{1}{2N} \ln \left(R + \sqrt{R^2 - 1} \right) \right]$$

The array factor evaluation through the Tchebyshev polynomial comes as the next step. The Tchebyshev polynomial approximation to the second order ($T_2(x)$) is sufficient so the current coefficients can be obtained, remembering that a symmetrical amplitude distribution hypothesis has been made. In this case the current coefficients C_i , $i \in \{-2, -1, 0, 1, 2\}$ follow the rule $C_i = C_{-i}$, thus their symbolic representation can be simplified as follows: C_n , $n \in \{0, 1, 2\}$ (or just $n = \overline{0, 2}$). Since the *Riblet variation* to the *Dolph-Tchebyshev synthesis model* has been used, the variable of $T_2(x)$ becomes $x = a + b \cos(u)$ and the formulation for $d_{opt} \in (\lambda/2, \lambda]$ differs from the standard model. The coefficients a and b are related to the maximum value selected in the sub-domain of $T_2(x)$ (the window of visible radiation lobes). This maximum, called for example x_1 , corresponds to the main lobe in which it can be converted by evaluating the array factor $|T_2(x_1)|$ (some additional references to the specific formulas that need to be used in order to compute can be found in [1] and [5]). That said, the current coefficients can be extracted from $T_2(x)$ (so by using eq. (2)). Resulting uniquely out of a C_n dependence, the tapering efficiency is obtained by using eq. (3).

Next, both non uniform amplitude (Tchebyshev array, *NUA*) and uniform amplitude (*UA*) cases are compared. The comparison shows how the BW_{fn} in the *UA* case (i.e. $BW_{fn}^{[UA]}$) is

narrower than that of *NUA* case (i.e. $BW_{fn}^{[NUA]}$). This result (see eq. (4) and table 2) is generally effective and the comparison has been made to show that this particular design case confirms the general condition.

All the numerical quantities related to the Tchebyshev array design are gathered together in table 2. After these quantities are calculated, some important design considerations can be made about the array efficiency. A Non-Uniform Amplitude Array Factor has been designed by using the Riblet variation of the Dolph-Tchebyshev array synthesis model. Considering the *maximum to minimum feed ratio*:

$$r_{\max/\min} = \frac{C_{\max}}{C_{\min}}$$

the less $r_{\max/\min}$ is, the more efficient distribution of current is reached. In this particular design, the requirement was to find the d_{opt} which minimizes the beamwidth, starting from the input design variables. Thus, the $r_{\max/\min}$ is a straight consequence of the current coefficients and its optimal value has not been the seek of this project. Anyway, for this design, $r_{\max/\min} \cong 4.39$ meaning that if a damage of the element with the C_{\max} (i.e. C_0) level of feed occurs, most part of the efficiency will be lost. In any case, the tapering efficiency shows how it will not be possible to take advantage of 21% of the array in an ideal situation, remembering that this design model can be discerned by the real circumstance in terms of the Tchebyshev error (see [1]).

$$\begin{aligned} T_2[x = a + b \cos u] &= \dots \\ &= C_0 + 2C_1 \cos u + C_2 \cos 2u \\ &= (2a^2 + b^2 - 1) + 4ab \cos u + b^2 \cos 2u \end{aligned} \quad (2)$$

$$\eta_T = \frac{1}{2N+1} \frac{\|C_0 + 2C_1 + 2C_2\|^2}{C_0^2 + 2C_1^2 + 2C_2^2} \quad (3)$$

$$BW_{fn}^{[UA]} < BW_{fn}^{[NUA]}$$

$$BW_{fn}^{[NUA]} = 2 \frac{180}{\pi} \left[\frac{\pi}{2} - \arccos \left(\frac{\arccos \left(\frac{\cos \left(\frac{\pi}{2N} - a \right)}{b} \right)}{k_0 d} \right) \right] \quad (4)$$

$$BW_{fn}^{[UA]} = \frac{2\lambda}{N d} \frac{180}{\pi}$$

In the end, the 2D array patterns resulting by the use of the calculated parameters are shown in fig. 1. Two polar patterns and their corresponding rectangular ones have been plotted (in the azimuth cut plane and in the elevation cut one).

Rectangular folded patch design

The main components of a rectangular folded patch are: the patch, the substrate (generally accessory, but used in this project), the ground, the rectangular shorting pin between the patch

Array factor input design variables	
Parameter	Value
# elements	$n_{el} = 2N + 1 = 5$
Mean lobe/side lobe ratio	$R = 120 \cong 41.58 \text{ dB}$
Frequency	$f = 2.1 \text{ GHz}$

Table 1: Table trial

Parameter	Value
Feed coefficients [A]	$C_0 = 41.2$ $C_1 = C_{-1} = 29.8$ $C_2 = C_{-2} = 9.6$
Normalized feed coefficients to C_{\max}	$C_0^* = 1.000$ $C_1^* = C_{-1}^* = 0.7215$ $C_2^* = C_{-2}^* = 0.2336$
Tapering efficiency	$\eta_T = 79\%$
Beamwidth	Tchebyshev 50.6° Uniform 34.8°

Table 2: Tchebyshev array design results

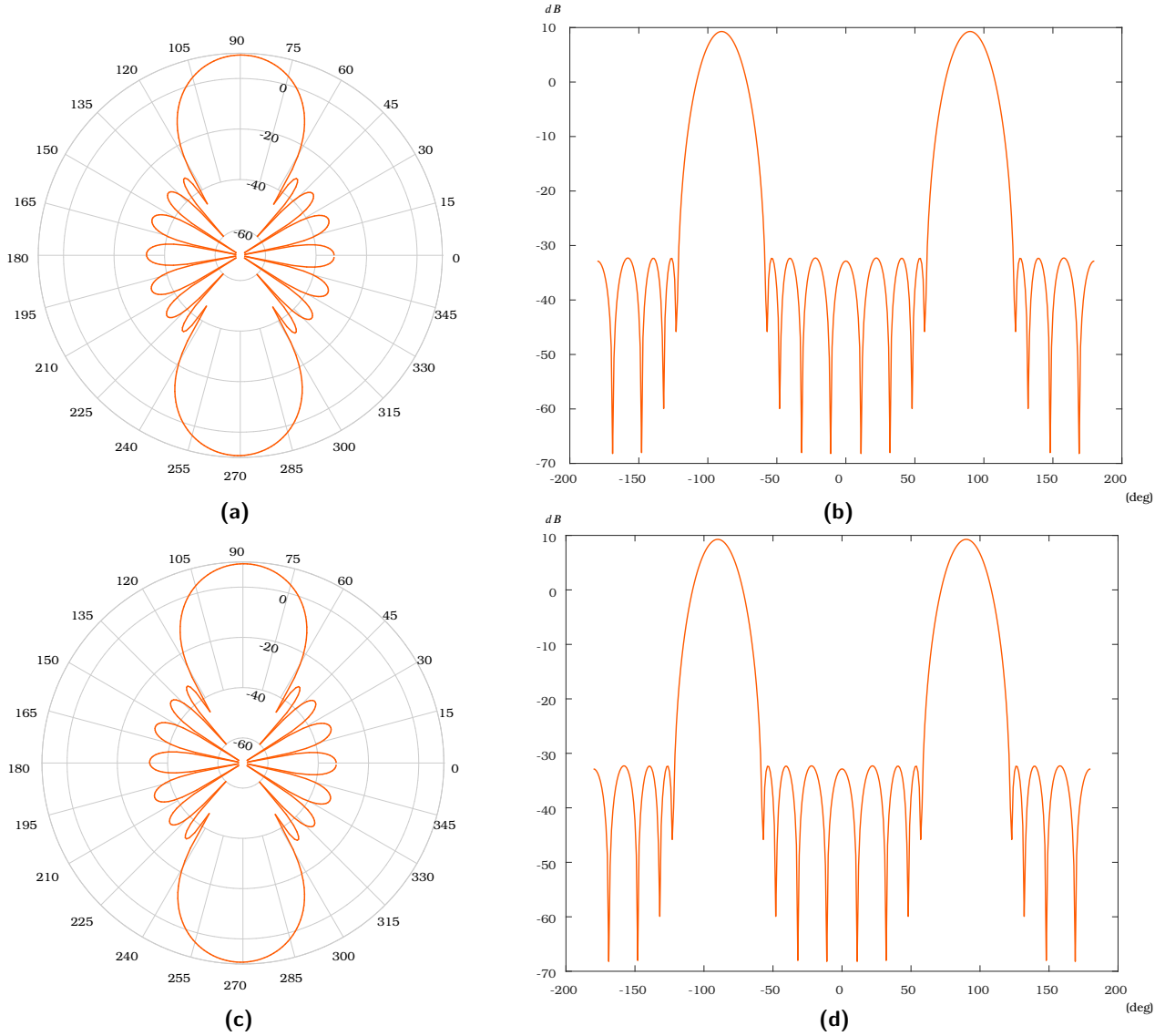


Figure 1: Array factor polar, in azimuth (a) and elevation (c) cut, and rectangular in azimuth (b) and elevation (d) cut, diagrams

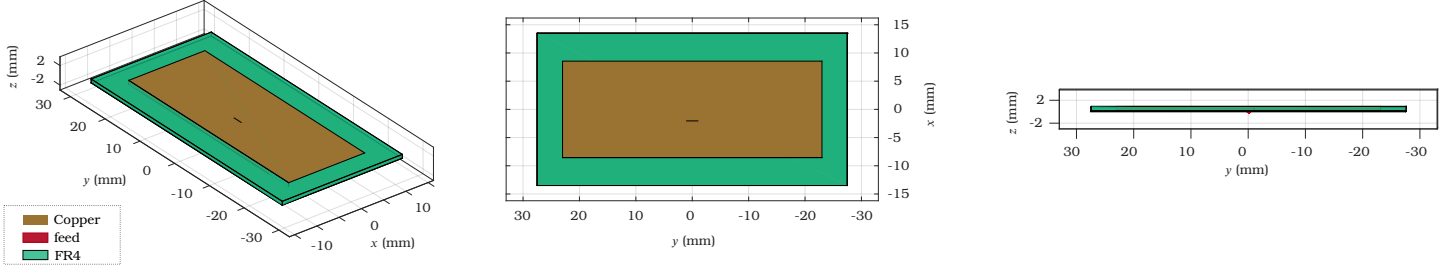
and the ground, and the feed. More details about them will be presented in a short while. Before that, some other remarks are necessary: this antenna will be the element of the array, which will be designed starting actually from a PIFA (*Planar Inverted F Antenna*), given the limitations of the [Antenna Toolbox](#), which will be discussed and overcome later on. A general PIFA realized with a dielectric substrate is shown in [fig. 2](#). A particular condition is imposed to the PIFA, by which the width of the rectangular shorting pin (w_{sc}) equals the patch width size (W_{patch}), so that the PIFA and the folded patch antenna will be two equivalent structures (see [eq. \(5\)](#)). This remark on the PIFA is necessary because generally its structure is not equivalent to that of the folded patch antenna because of the possible variability of the shorting width (w_{sc}), which doesn't always satisfy the above imposed condition. This condition on w_{sc} represents one of the input variables of the PIFA design, such as the matched input resistance (R_{in}), the resonant frequency (f) and the substrate characteristics (see [table 3](#)). A preliminary evaluation of the patch parameters have been realized by leaning on a theoretical set of formulas (see [\[1\]](#)). That's the reason why the characteristics of the patch shown into the [table 3](#) are called "pre-optimized features" (same thing applies

to the ground component). Thus, an optimization process of all these and other parameters will be performed in some following steps. Just before that, now the theoretical model will be shortly pointed out: it furnishes a provisional set of results (that will be adjusted afterward). Firstly length and the width of the patch starting from the $w_{sc} = W_{patch}$ imposed condition, the substrate wavelength and thickness (i.e. λ_{FR4} and h_{FR4}) are calculated ([eq. \(6\)](#)). Then, other parameters, such as the effective permittivity ϵ_{eff} and length (L_{eff}) in [eq. \(7\)](#), the radiation resistance (R_r) in [eq. \(8\)](#), the half-power beamwidth in the E-cut (Θ_E) and the H-cut (Θ_H) in [eq. \(9\)](#) and eventually the feed location (ℓ_{feed}) in the patch length direction with respect to the free edge ([eq. \(10\)](#)) have been calculated.

Refinement with MatLab MoM

Substrate thickness selection

Three thickness levels were available for the *FR4* substrate required in this project (see [table 4](#)). In this part it will be explained why choosing a thinner substrate (if the *FR4* is used) is more convenient. This choice will be motivated both in relation

**Figure 2:** PIFA realized with a dielectric substrate

to the physical behaviour (radiation efficiency) and to the limits of the **Matlab** tools that have been used (in terms of the mesh density level selection in a range that gives more reliable results).

FR4 substrate project thickness available (mm)		
$h_{FR4}^{(1)} = 0.8$	$h_{FR4}^{(2)} = 1.0$	$h_{FR4}^{(3)} = 1.6$

Table 4: Three levels of *FR4* substrate thickness are shown above. In the antenna industry, the *FR4* substrate thickness generally ranges from 0.8 mm and 3.6 mm

$$W_{patch} = w_{sc} \quad (5)$$

$$\begin{aligned} L_{patch} + W_{patch} - w_{sc} &= \frac{\lambda_{FR4}}{4} + h_{FR4} \\ W_{patch} &= \frac{\lambda}{2} \sqrt{\frac{2}{\epsilon_{FR4} + 1}} \end{aligned} \quad (6)$$

$$\begin{aligned} \epsilon_{eff} &= \frac{\epsilon_{FR4} + 1}{2} + \frac{\epsilon_{FR4} - 1}{2} \left(1 + 12 \frac{h_{FR4}}{W_{patch}} \right)^{-\frac{1}{2}} \\ L_{eff} &= \frac{\lambda_{FR4}}{4} \\ \Delta L &= 0.412 h \left[\frac{(\epsilon_{eff} + 0.3) \left(\frac{W_{patch}}{h_{FR4}} + 0.268 \right)}{(\epsilon_{eff} - 0.258) \left(\frac{W_{patch}}{h_{FR4}} + 0.8 \right)} \right] \\ L &= L_{eff} - 2\Delta L \end{aligned} \quad (7)$$

$$R_r = \frac{120 \lambda}{W_{patch}} \left[1 - \frac{1}{24} \left(2\pi \frac{h_{FR4}}{\lambda} \right)^2 \right]^{-1} \quad (8)$$

$$\begin{aligned} \Theta_E &= 2 \arccos \sqrt{\frac{7.03 \lambda^2}{4(3L_e^2 + h_{FR4}^2)\pi^2}} \\ \Theta_H &= 2 \arccos \sqrt{\frac{1}{2 + 2\pi \frac{W_{patch}}{\lambda}}} \end{aligned} \quad (9)$$

$$\ell_{feed} = \frac{L_{patch}}{\pi} \arccos \sqrt{\frac{R_{in}}{R_r}} \quad (10)$$

$$\begin{aligned} h_{FR4} = 0.8 \text{ mm} &\rightsquigarrow h_\lambda = \frac{1}{81} \\ h_{FR4} = 1.0 \text{ mm} &\rightsquigarrow h_\lambda = \frac{1}{62} \end{aligned} \quad (11)$$

Folded patch design parameters	
Parameter/Component	Value/Type/Material
Frequency	2.1 GHz
Matched input resistance	$R_{in} = 50 \Omega$
Substrate	FR4
Relative permittivity	$\epsilon_{FR4} = 4.8$
Relative permeability	$\mu_{FR4} \cong 1$
Loss tangent	$\{\tan(\delta)\}_{FR4} = 0.0260$
Thickness	$h_{FR4} = 0.8 \text{ mm}$
Patch (pre-optimized features)	Copper
Conductivity	$\kappa_{copper} = 5.96 \cdot 10^7 \text{ S/m}$
Thickness	$h_{patch} = 3.556 \cdot 10^{-5} \text{ m}$
Length	$L_{patch} \cong \frac{\lambda_{FR4}}{4} = 0.0171 \text{ m}$
Width	$W_{patch} \cong 0.419 \text{ m}$
Ground (pre-optimized features)	Copper (same conductivity listed above)
Thickness	$h_{GND} = h_{patch}$
Length	$L_{GND} = 0.04 \text{ m}$
Width	$W_{GND} = 0.06 \text{ m}$
Feed	Coaxial cable

Table 3: Project input parameters (frequency, matching and substrate features) and theoretical (pre-optimized) features of the patch and ground PIFA components

The **Antenna Toolbox** gives specific information about the mesh density level that should be adopted for the design of the patch antenna components. The only issue is that these details are given only for particular ranges of the ratio indicator called *relative thickness* or *electrical thickness* h_λ (see [2]). The electrical thickness depends on the ratio between the substrate thickness (h_{FR4}) and the wavelength related to the substrate medium (λ_{FR4}). When a mesh is configured in the **Antenna Toolbox** environment, a specific parameter needs to be adjusted: the maximum edge length of the generic triangle covering the geometry of the antenna (e_{max}). In the case of a relative length h_λ comparable to 1/10, it's recommended to select an

$e_{\max} \cong \lambda/10$. A substrate thickness respecting this relationship is called a *thick substrate*. None of the available substrates verifies this condition. Among them, only the thinnest substrate and the second to last one (thus $h_{FR4} = 0.8 \text{ mm}$ and $h_{FR4} = 1.0 \text{ mm}$) are part of a range which the [Antenna Toolbox](#) provides instructions of. It's the *thin substrate range*: the automatic mesh mode should be adopted for a thin substrate, namely having a relative thickness less or equal than one fifth ($h_\lambda \leq 1/50$). An evaluation of the h_λ of two substrates respecting this condition is shown in [eq. \(11\)](#). This leads to a full explanation of actual substrate thickness chosen for this project. The thinner substrate choice rationale starts with the consideration of its quality factor (Q) depending on the loss tangent ($\tan\delta$) is generally low in the FR4 substrate case (being the two quantities inversely proportional, i.e. $Q \propto 1/\tan\delta$, and being $(\tan\delta)$ very high compared to that of other more efficient substrates). This means the FR4 is a big power disperser. Since increasing h_{FR4} will provoke just more losses in terms of a radiation efficiency drop and since the only thickness values of 0.8 mm and 1.0 mm would give reliable/accurate results in the [Antenna Toolbox](#) simulations, the 0.8 mm thickness level will be adopted.

Mesh density refinement

Although a mesh density choice has already been made by selecting the best maximum edge length e_{\max} , the accuracy achievable by using the mesh automatic mode in the case of substrates belonging to the *thin substrate range* will be proved hereafter. An initial study of the mesh density level influence on the reflection coefficient (Γ in dB) evaluated at the resonant frequency ($f = 2.1 \text{ GHz}$) has been realized, thus a $\Gamma_{2.1 \text{ GHz}} = F(e_{\max})$ function has been plotted with an initial step of $\Delta e_{\max} = 2.5 \cdot 10^{-4} \text{ m}$ between every two mesh densities related to their specific e_{\max} . This first simulation considered a broader range of e_{\max} variation: $[2.5 \cdot 10^{-4} \text{ m}, 6.0 \cdot 10^{-4} \text{ m}]$.

Since the resulting plot ([fig. 3](#)) has shown big uncertainty of the reflection coefficient value at the resonant frequency ($\Gamma_{2.1 \text{ GHz}}$) at almost every mesh e_{\max} level (primarily due to the big step selected between one density level and another), some more detailed tests have been run, by considering a slightly narrower range ($[2.5 \cdot 10^{-4} \text{ m}, 5.0 \cdot 10^{-4} \text{ m}]$) and a thicker evaluation of the maximum edge values (so that the mesh variation step has been remarkably reduced to $1.0 \cdot 10^{-4} \text{ m}$). Specifically, the step between two mesh density levels in terms of the maximum edge length of each one has been reduced from a $\Delta e_m = 2.5 \cdot 10^{-4}$ to $\Delta e_m = 1.0 \cdot 10^{-4}$. In all those simulations, an important fact needs to be noted. Even very small variations on the maximum edge length value involved considerable inconsistencies in almost every part of the mesh range in terms of considerable variations of the frequency at which Γ reaches its minimum ($\min(\Gamma)$), therefore the resonant frequency of the antenna changes very easily). Thus, considering the frequency f^* at which $\min(\Gamma)$ is actually obtained, instead of evaluating it at the theoretical resonating frequency value at every mesh level, not only the standard test comparing e_{\max} and Γ has been run, but also some mesh refinement plots representing the relationship between f^* and e_{\max} ([fig. 4c](#)), Δf^* and e_{\max} ([fig. 4b](#)) and also $\min(\Gamma)$ and e_{\max} ([fig. 4a](#)) have been taken into account (where Δf^* is the difference between f^* and the res-

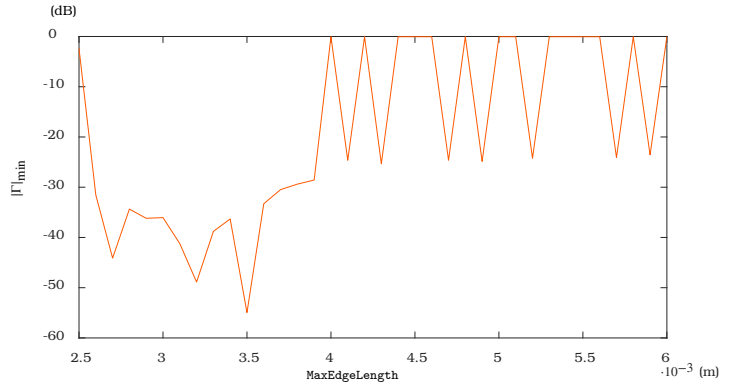


Figure 3: Minimum of the reflection coefficient $\Gamma[\text{dB}]$ in the frequency range $2.0 \div 2.2 \text{ GHz}$ depending on the varying mesh density level

Parameter	Value
Γ_{final}	-54.94 dB
R_{in}	49.86Ω
Y_{in}	0.11 S

Table 5: Final Γ and impedance matching values after w_{feed} change

onant frequency $f = 2.1 \text{ GHz}$). More parameter relationships have been collected and this led to the setting of the mesh density choice in terms of e_{\max} that has been selected inside the most stable region (i.e. showing the smallest deviation of the reflection coefficient minimum from the resonant frequency). In the end it's been specifically taken the 'automatic' e_{\max} ($= 3.5 \cdot 10^{-4} \text{ m}$) suggested by the [Antenna Toolbox](#), since this value belongs to the stable region and seems to give the most accurate results. The e_{\max} values belonging to the stable region ($[3.1 \cdot 10^{-4} \text{ m}, 3.7 \cdot 10^{-4} \text{ m}]$) exhibit slight deviations from the resonant frequency ($\Delta f^* \in [0.01 \text{ GHz}, 0.03 \text{ GHz}]$) and the minimum of the reflection coefficient varies in the range $[-24 \text{ dB}, -33 \text{ dB}]$.

Patch parameters refinement

After the selection of the maximum edge length of the mesh (consequently, of its density level), a more refined computation of the reflection coefficient will be made, depending on the patch size (i.e. on its length and width), but also on the feed location. Firstly, only a parametrical variation of the feed position across the patch length direction has been considered, depending on variations of L_{patch} and W_{patch} . This means that the first refinement of the feed position has been evaluated starting from its theoretical equation (depending indirectly by W_{patch}). The change of the feed location has been taken into account in the computation of every step of the simulation, thus in every evaluation of the reflection coefficient, keeping e_{\max} as a constant (the previously selected length). The patch size variations provoked wide modifications of the reflection coefficient, which values depending on that have been represented by an initial contour plot (with variations of the patch size in a broader range and with a larger step between one value and another, see [fig. 6a](#)). After that, another simulation ([fig. 6b](#)) in a narrower range of the

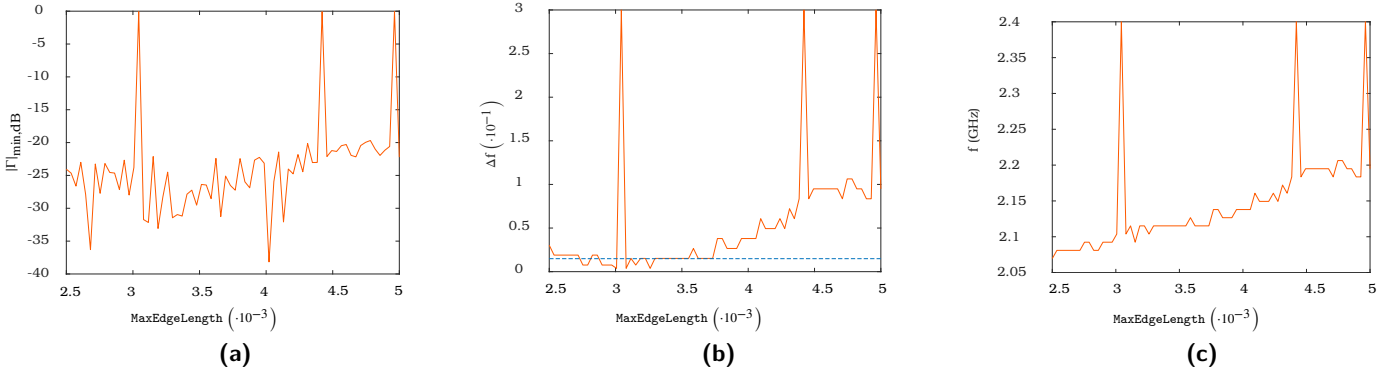


Figure 4: Comparison of the meshing parameter e_{\max} with minimum of reflection coefficient (a), variation of the resonant frequency with respect to the design one (the dotted line represents the value with respect to automatic meshing) (b), resonant frequency identified by the minimum of Γ (c)

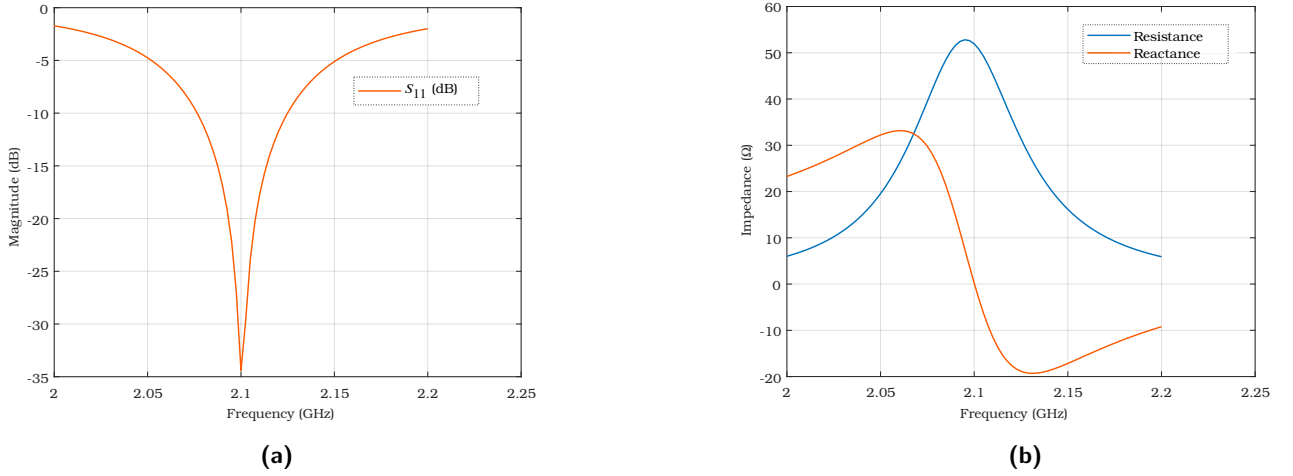


Figure 5: Reflection coefficient (a) and impedance (b) plots depending on $f \in [2.0, 2.1] \text{ GHz}$

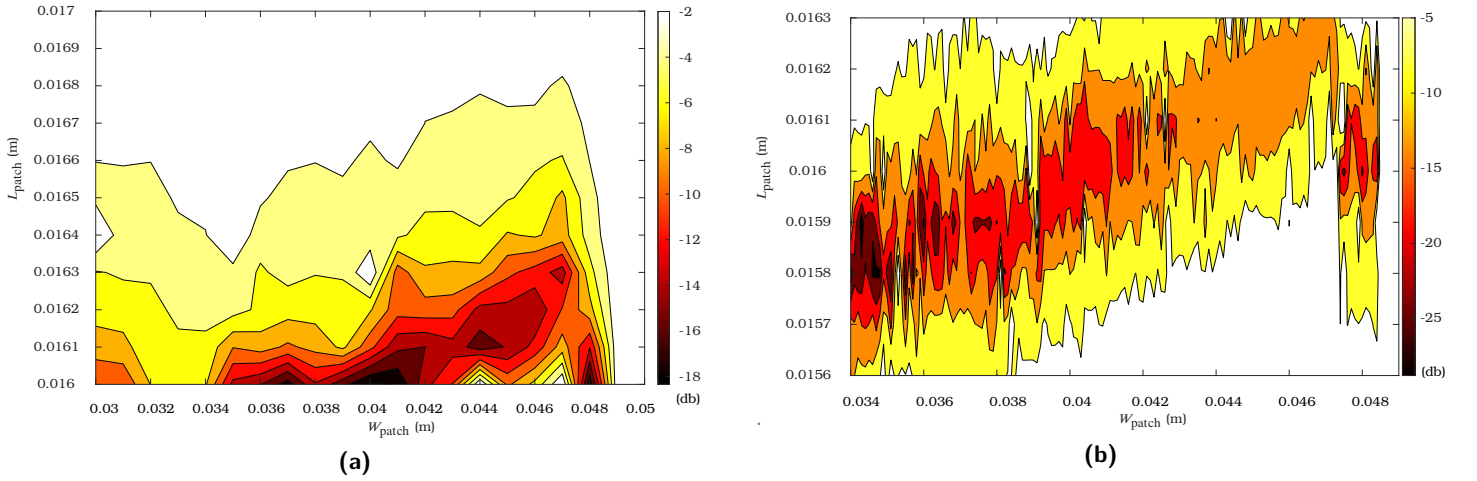


Figure 6: First (a) and second (b) contour plots depending on the patch size (L_{patch} and W_{patch} variations)

patch size variation has been run in order to choose from there a set of Γ values (i.e. a set of coupled values (L_{patch}, W_{patch})) that should put the patch antenna in the best resonant condition (which means that a Γ as close as possible to zero in the linear

scale and as negative as possible in the dB , logarithmic scale is sought). The logarithmic (dB scale) was used for the contour plots because this way the resulting Γ values are easier to distinguish from one another even graphically and mathematically.

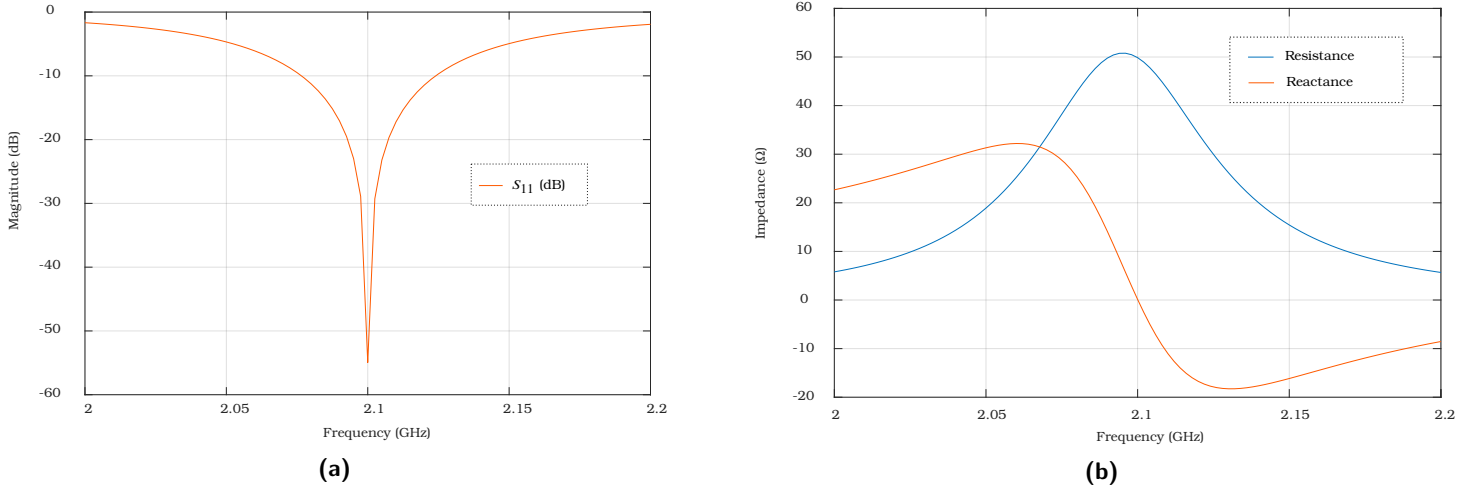


Figure 7: Final Γ (a) and impedance matching (b) plots after further refinement including w_{feed} change

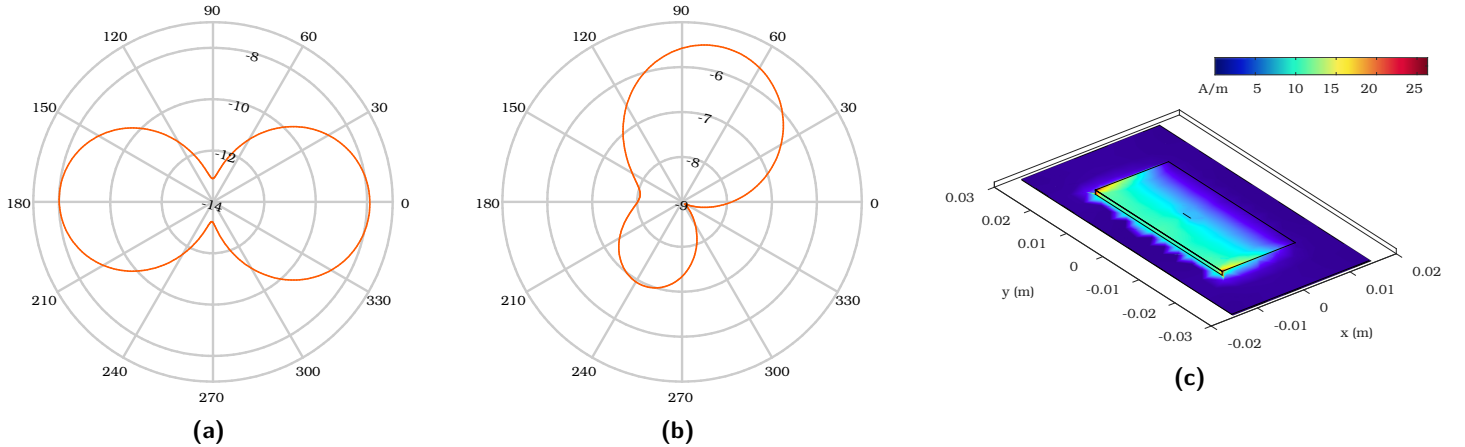


Figure 8: Gain patterns (a) in 3D, (b) in the null elevation plane, (c) in the null azimuth plane and (d) 3D current plot on the patch antenna

A set of 20 values of Γ and respective coupled values (L_{patch}, W_{patch}) has been selected from the second simulation range so that a more specific simulation could be run. In this third case (fig. 10), the reflection coefficient has been plotted in a range around the resonant frequency ([2.0 GHz, 2.2 GHz]) in order to find which is the best combination for the patch size that makes actually resonate the antenna at the project frequency. Another determining and discriminating factor was the input impedance ($Z_{in} = R_{in} + jY_{in}$, where the real part of Z_{in} is the input resistance, while the imaginary one is the input reactance), because a impedance matching (at 50 Ω) needed to be achieved for the project. In the ideal case, of course, a reflection coefficient $\Gamma^{(id)} = 0.00 \rightarrow -\infty$ dB would be required in order to reach the perfect impedance matching (perfect matching with input resistance at 50.00 Ω and null reactance). As an actual result, before seeking a better matching, the Γ value related to all the couple candidates ((L_{patch}, W_{patch})) spaced ranged from -24 dB to -30 dB. The two best candidates of the Γ value related to the coupled size (L_{patch}, W_{patch}) are plotted in fig. 10. Two refined plots (with narrower frequency steps in the same range) of Γ and Z for one of the candidates are represented in fig. 5. An additional design strategy contributed to the final patch size choice: the feed location varying across the patch width direction (w_{feed}). Thus, a parametrical impedance matching study

depending on that has been run on the best couple candidates and a few others from the set of 20. The resulting values are listed in table 5 and the plots are shown in fig. 7

From the PIFA to a PCB stack approximation Since the **Antenna Array Designer** is not able to generate an array of PIFAs, the **Sensor Array Analyzer** has been used to create that type of structure, starting from the Tchebyshev array factor design made in the first part and from the previous optimization process of a single PIFA. In the last part the overall array of PIFAs needs to be analyzed by means of beamsteering for particular angles, total gain, electric and magnetic field patterns. Unfortunately, not all of this information can be extracted by using uniquely the **Sensor Array Analyzer** tool. This fact led to the use of another tool, the **PCB Antenna Designer**, so that all the parameters required for the project could be analyzed. With this last tool, a similar structure to that of the PIFA has been realized and introduced as the antenna element of the array distribution. Just before moving to the array analysis, a comparison between the single antenna being a PIFA structure and the antenna created by using a PCB stack was performed. A single limitation in the use of the **PCB Antenna Designer** has been encountered, but it has been overcome with an approximation strategy. Thus, the PIFA and the PCB stack designed

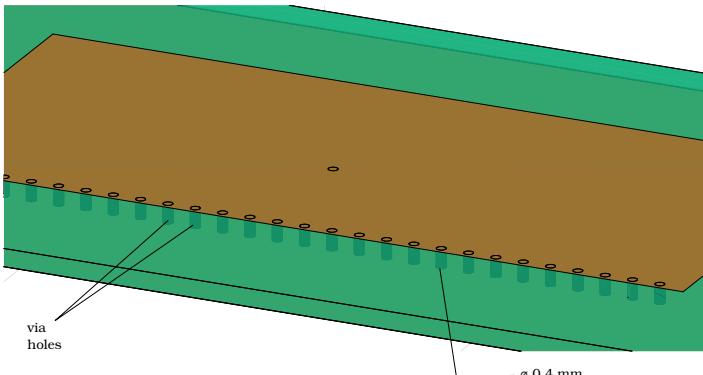


Figure 9: Cropped zoom over PCB via holes. For an overall picture see fig. 11

are not perfectly identical, but their single and overall performance inside the array had shown a slight quantifiable difference. The limitation consisted in the absence of a specific option or combination of commands that would allow to realize the rectangular shorting pin between the patch and the ground. The only thing the designer can do is to replace this kind of shorting pin with a series of small diameter (e.g. 0.4 mm) cylindrical shorting pins (see **fig. 11**) and **fig. 9** close to one edge of the patch, across the patch width direction. With this design choice, a very similar behaviour to that of the PIFA structure was possible to simulate. To support this results, a comparison of the 2D gain patterns (elevation and azimuth cut) of the PIFA to those of the PCB stack antenna has been realized in terms of the mean square error values, shorten MSE , related to the two specific two-dimensional patterns considered (MSE_{el} in the elevation cut directivity pattern and MSE_{az} in the azimuth cut directivity pattern). Furthermore, since the **Sensor Array Analyzer** allows the plotting of some patterns such as the directivity (but not of the gain), a comparison between the 2D patterns of the antenna array of PIFAs and the array of PCBs has been presented. In that case the error is presented as a comparison between the main lobe levels in the PIFA array and the PCB array cases, but also in terms of a first side lobe levels of the two arrays. This discussion was necessary, because moving to the last part of the project required a deeper study of the array of antennas, that will be displayed by using the PCB antenna as the element of the array.

Overall patch antenna array performance

In this last part of the project, the array factor and the element antenna (PIFA or PCB stack) designs will be combined so that their total effect will be examined. As it's been already mentioned in the previous paragraph, some of the information describing the overall array performance can be asked from both the **Sensor Array Analyzer** (where the array of PIFAs was designed) and the **PCB/Antenna Array Designer** (where the single patch antenna made starting from the PCB stack and also the whole array can be constructed). The performance of the overall array will be evaluated in two cases: in the broadside case (90°) but also at 45° off the boresight direction. First of all, it is very simple to identify the phase shift coefficients in the broad-

side case because they all equal 0° (there's no actual phase shift between antennas). In the second case, some manual calculation can be made in order to insert the phase shifts between the single antennas (this is the case of the PCB stack array), and it can be also automatically computed by using the array of PIFAs. The generic procedure is shown in **eq. (13)**. Just before moving to the last part of the analysis, where only the characteristics of the array of PCBs will be considered, a last comparison between the array of PCBs and the array of PIFAs will be made in terms of 2D directivity patterns (both in broadside and in 45° off the boreside direction, see **fig. 15**). An error analysis based on the difference between the PCBs array main lobe and that of the PIFAs array, but also on the difference between the PCBs array main side lobe and that of the PIFAs array will be shown. The patterns and the numerical results according to the numerical error values illustrate how the array of PCBs represent a good enough approximation of the array of PIFAs.

Total array gain

In order to get and describe the last plots of the project, it is not possible to recur to the **Sensor Array Analyzer** because some of the commands, such as **EHfields** and **patternMultiply**, are not available in this tool. Thus, in this last part, only the array of PCBs will be used, because it's compatible with these commands. The total array gain will be computed and displayed in two different cases: by means of a full-wave model (with no approximation) and by using the pattern multiplication principle. This second case is idealistic because it makes an approximation of the real patterns by not considering the mutual induced interactions between the single antennas of the array; however, a "mathematical" interaction is considered in this model because it comes out of a formulation that mixes the single element effect (which gives an element gain factor G_0) on the gain pattern with the angular filtering influence of the array factor, weighted by a combination of the current coefficients (which gives an array gain factor G_F). The overall idealistic case is based on the pattern multiplication principle, which (in a case such as the Tchebyshev array synthesis model, thus with non uniform amplitude feed), will take into account also the effect of the tapering efficiency (η_T) in its formulation (see **eq. (14)**). Thus, the pattern multiplication principle can be applied angle by angle and this will provide a set of values that can be computed and inserted in matrices by using **MatLab**. Starting from the matrices, the 2D patterns can be represented. On the other hand, an easier way is to use the **patternMultiply** command and get the ideal patterns.

Electric and magnetic near fields

The near field characteristics (specifically those of the radiative field, also called the Fresnel region) have been analyzed in both the broadside and by beamsteering to 45° off the boresight conditions. Two situations have been analyzed: the general near field behaviour (in its electric and magnetic field components) but also the specific orientation of the fields in the center position of each of the five elements composing the antenna (so considering the x and y coordinates of each patch corresponding to the length and width directions of its planar development and the z coordinate representing the vertical component of the dis-

Direction	$D_{ML,az}$ error		$D_{SL,az}$		$D_{ML,el}$ error		$D_{SL,el}$	
Broadside (90°)	ΔD_{ML}	$\Delta D_{ML}^r \%$	ΔD_{SL}	$\Delta D_{SL}^r \%$	ΔD_{ML}	$\Delta D_{ML}^r \%$	ΔD_{SL}	$\Delta D_{SL}^r \%$
	2.39 dB	3.3 %						
Off Boresight (45°)	ΔD_{ML}	$\Delta D_{ML}^r \%$	ΔD_{SL}	$\Delta D_{SL}^r \%$	ΔD_{ML}	$\Delta D_{ML}^r \%$	ΔD_{SL}	$\Delta D_{SL}^r \%$
	0.05 dB	0.07 %						

Table 6: Comparison between the array of PIFAs and the array of PCBs in terms of the directivity evaluated in their main lobes and first side lobes, both in the broadside and 45° off the boresight direction, both in the azimuth cut (*az*) and elevation cut (*el*) planes. The comparison has been made in terms of the directivity difference ($\Delta D_{\#} = D_{PIFAs} - D_{PCBs}$ in dB) in the corresponding positions and also as a relative percentage error ($\Delta D_{\#}^r \%$, the ratio between $\Delta D_{\#}$ and the directivity in the array of PIFAs case (D_{PIFAs}))

$fre \leftrightarrow$ Fresnel region $fraun \leftrightarrow$ Fresnel region	Position	<i>E</i> -field (90°)	<i>H</i> -field (90°)	<i>E</i> -field (45°)	45-field (90°)
PCB fed by C_{-2}	(0, $-2d_{opt}, z_{fre}/2$)	0.1027	0.0139	0.2071	0.0269
	(0, $-2d_{opt}, z_{fraun}/2$)	0.0848	0.0114	0.2071	0.0269
	(0, $-2d_{opt}, 4z_{fraun}$)	0.0161	0.0020	$0.1651 \cdot 10^{-3}$	$0.1360 \cdot 10^{-3}$
PCB fed by C_{-1}	(0, $-d_{opt}$)	0.2923	0.0377	0.1889	0.0100
	(0, $-d_{opt}, z_{fraun}/2$)	0.1144	0.0143	0.1889	0.0100
	(0, $-d_{opt}, 4z_{fraun}$)	0.163	0.0020	$0.1493 \cdot 10^{-3}$	$0.1365 \cdot 10^{-3}$
Mid PCB, fed by C_0	(0, 0, $z_{fre}/2$)	0.4189	0.0522	0.2422	0.0174
	(0, 0, $z_{fraun}/2$)	0.1258	0.0155	0.2492	0.0174
	(0, 0, $4z_{fraun}$)	0.163	0.0020	$0.1285 \cdot 10^{-3}$	$0.1364 \cdot 10^{-3}$
PCB fed by C_1	(0, $d_{opt}, z_{fre}/2$)	0.3306	0.0367	0.2619	0.0215
	(0, $d_{opt}, z_{fraun}/2$)	0.1191	0.0145	0.2619	0.0215
	(0, $d_{opt}, 4z_{fraun}$)	0.162	0.0020	$0.1053 \cdot 10^{-3}$	$0.1357 \cdot 10^{-3}$
PCB fed by C_2	(0, $2d_{opt}, z_{fre}/2$)	0.1350	0.0143	0.2922	0.0270
	(0, $2d_{opt}, z_{fraun}/2$)	0.0971	0.0116	0.2922	0.0270
	(0, $2d_{opt}, 4z_{fraun}$)	0.162	0.0020	$0.0744 \cdot 10^{-3}$	$0.1343 \cdot 10^{-3}$

Table 7: Particular electric (*E*) and magnetic (*H*) field values measured in both broadside (90°) and in the 45° off the boresight directions. The *E*-field is measured in $\left[\frac{V}{m} \right]$ while the *H*-field in $\left[\frac{A}{m} \right]$. The fields have been measured with respect to the centers of each element antenna vertically off the array plane at different height levels of z_{fre} (inductive region), z_{fraun} (radiative region) and $4z_{fraun}$ (particular coordinate in the far field region).

tance between the observation point and the array. The vertical distance z has been considered in three different cases. First, the Fresnel region (inductive near field region) has been analyzed at $z_{fre} = 0.62\sqrt{L_{max}^3/\lambda}$ (where L_{max} is the maximum size of the array, thus $L_{max} = 4d_{opt} + L_{patch}$), while the inductive near field region was measured, starting from the Fraunhofer limit expression (z_{fraun}), at $z_{fraun}/2$. Moreover, it's been considered an observation point at a generic distance from the array in the far field region ($4z_{fraun}$). The three cases can be compared both in the broadside and in the 45° off the boresight direction examples. In the broadside case, the inductive and radiative near electric and magnetic fields can be ordered by following the increasing of their intensities as a criterion. It can be noted that the order of these intensities (calling them E_i , H_k , with $i, j = -2, 2$) is the same of that of the feed currents (the relationship is shown or the *E* field intensities - see eq. (12) - but it works analogously for the *H* field). In the far field, a totally different phenomenon is observable (at least in the broadside case and with good approximation in the 45° direction too): the *E*

field components are all equal, as those relative to the magnetic field *H*. This can be interpreted as follows: in the near field, the elements of the array still don't behave completely as one radiating object so that their individual radiative effect can be observed, prevailing on the mutual interactions that will make them work as a whole at a further distance (i.e. in the far field). This fact can be explicitly analyzed by looking at the electric and magnetic fields registered at the specific distances: everything is shown in ...

$$\begin{array}{ll}
 \text{If} & C_0 > C_1 > C_2 \\
 \text{and} & C_0 > C_{-1} > C_{-2} \\
 \text{then} & E_0 > E_1 > E_2 \\
 \text{then} & E_0 > E_{-1} > E_{-2}
 \end{array} \tag{12}$$

Methods

In this conclusive paragraph, a list of the **MatLab** commands that are not available for all the tools that have been used will

be pointed out. Next, the computational costs related to the different parts of the project will be discussed. In the end, a comparison between the array of PIFAs realized in **Matlab** and the **CST Studio Suite (Student edition)** will be shown.

Explaining what are the limitations of every tool and our previous suggestions about how to combine them (this made it possible to get conclusive results) may help the reader who wants to engage himself into doing some similar studies about array of antennas. Four different **MatLab** tools belonging to two different toolboxes have been used for this project. Through **Antenna Designer** to PIFA structure has been generated and analyzed, while the PCB stack has been created and studied through the **PCB Antenna Designer** and we got the array of PCBs out of the **Antenna Array Designer**. All these tools belong to the **Antenna Toolbox ([3])**, while the **Sensor Array Analyzer** (by which the study of the array of PIFAs is possible) is part of the **Phased Sensor Array Analyzer ([4])**.

$$\begin{aligned} u_0 = \alpha d_{opt} &= 2\pi \frac{d_{opt}}{\lambda} \cos(\theta_0) \\ \alpha_n = n \alpha d_{opt} &= nu_0 \quad (n = \overline{1, 5}) \end{aligned} \tag{13}$$

$$G_{total} = \eta_T G_0 G_T \tag{14}$$

Conclusion

Data availability

References

- [1] Constantine A. Balanis. *Antenna Theory: Analysis and Design*. John Wiley & Sons Inc, 2016.
- [2] Sergey N. Makarov. *Antenna and EM modeling with MATLAB*. A John Wiley & Sons, Inc., publication, 202.
- [3] MathWorks®. *Antenna Toolbox*. 2022. URL: <https://it.mathworks.com/products/antenna.html> (visited on 11/01/2022).
- [4] MathWorks®. *Phased Array System Toolbox*. 2022. URL: <https://it.mathworks.com/products/phased-array.html> (visited on 11/01/2022).
- [5] Sophocles J. Orfandis. *Electromagnetic Waves and Antennas*. The MathWorks, Inc., 1999-2016.

List of Figures

1	Array factor polar, in azimuth (a) and elevation (c) cut, and rectangular in azimuth (b) and elevation (d) cut, diagrams	3
2	PIFA realized with a dielectric substrate	4
3	Minimum of the reflection coefficient $\Gamma [dB]$ in the frequency range $2.0 \div 2.2 GHz$ depending on the varying mesh density level	5
4	Comparison of the meshing parameter e_{max} with minimum of reflection coefficient (a), variation of the resonant frequency with respect to the design one (the dotted line represents the value with respect to automatic meshing) (b), resonant frequency identified by the minimum of Γ (c)	6
5	Reflection coefficient (a) and impedance (b) plots depending on $f \in [2.0, 2.1 GHz]$	6
6	First (a) and second (b) contour plots depending on the patch size (L_{patch} and W_{patch} variations)	6
7	Final Γ (a) and impedance matching (b) plots after further refinement including w_{feed} change	7
8	Gain patterns (a) in 3D, (b) in the nulle elevation plane, (c) in the null azimuth plane and (d) 3D current plot on the patch antenna	7
9	Cropped zoom over PCB via holes. For an overall picture see fig. 11	8
10	The two best Γ plots depending on the specific patch size expressed coupled variations (L_{patch}, W_{patch}) and represented in a frequency range of $[2.0, 2.1] GHz$	12
11	3D view and top view of the PIFA approximation realized with a PCB stack and cylindrical shorting pins	12
12	Gain pattern for PIFA (a) !!!! SOSTITUIRE QUESTI PATTERN CON GLI ALTRI !!!	13
13	PIFA and PCB single antenna directivity patterns (dB) in the Azimuth cut ($\theta_{el} = 0^\circ$, (a)) and in the Elevation cut ($\phi_{az} = 0^\circ$, (b))	14
14	PIFA and PCB arrays directivity patterns (dB) in the Azimuth cut ($\theta_{el} = 0^\circ$, (a)) and in the Elevation cut ($\phi_{az} = 0^\circ$, (b))	14
15	2D patterns in both the broadside case ((a) azimuth cut and (b) elevation cut) and 45° off the boresight direction ((c) azimuth cut and (d) elevation cut).	15
16	17

Appendix

Figures

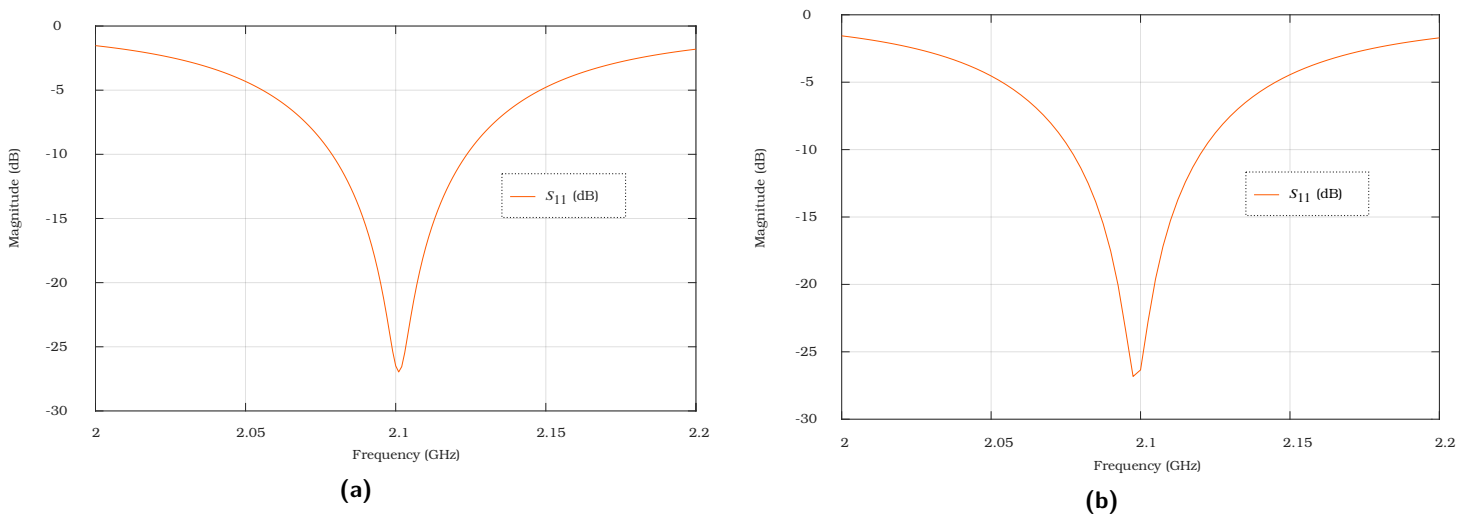


Figure 10: The two best Γ plots depending on the specific patch size expressed coupled variations (L_{patch}, W_{patch}) and represented in a frequency range of [2.0, 2.1] GHz.

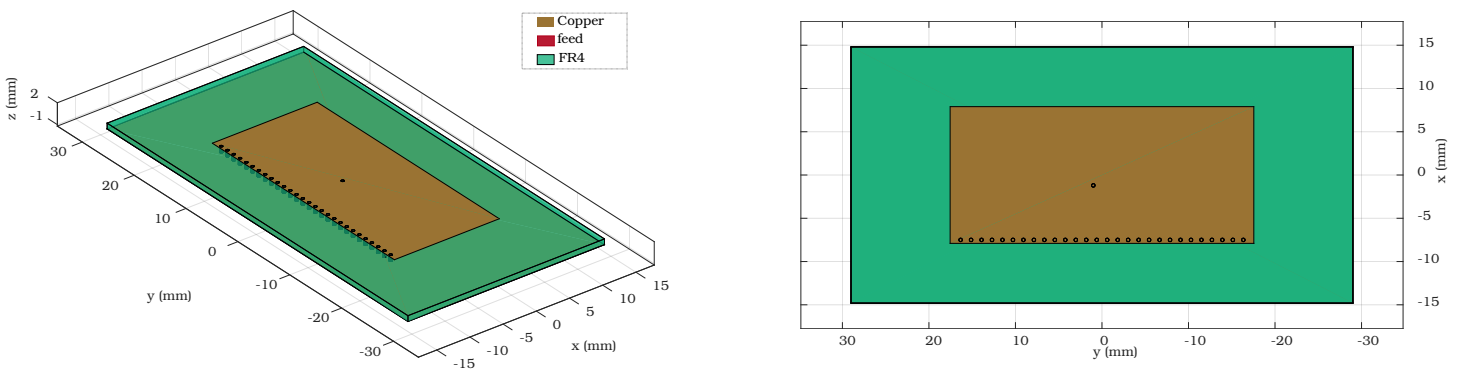


Figure 11: 3D view and top view of the PIFA approximation realized with a PCB stack and cylindrical shorting pins

Pattern

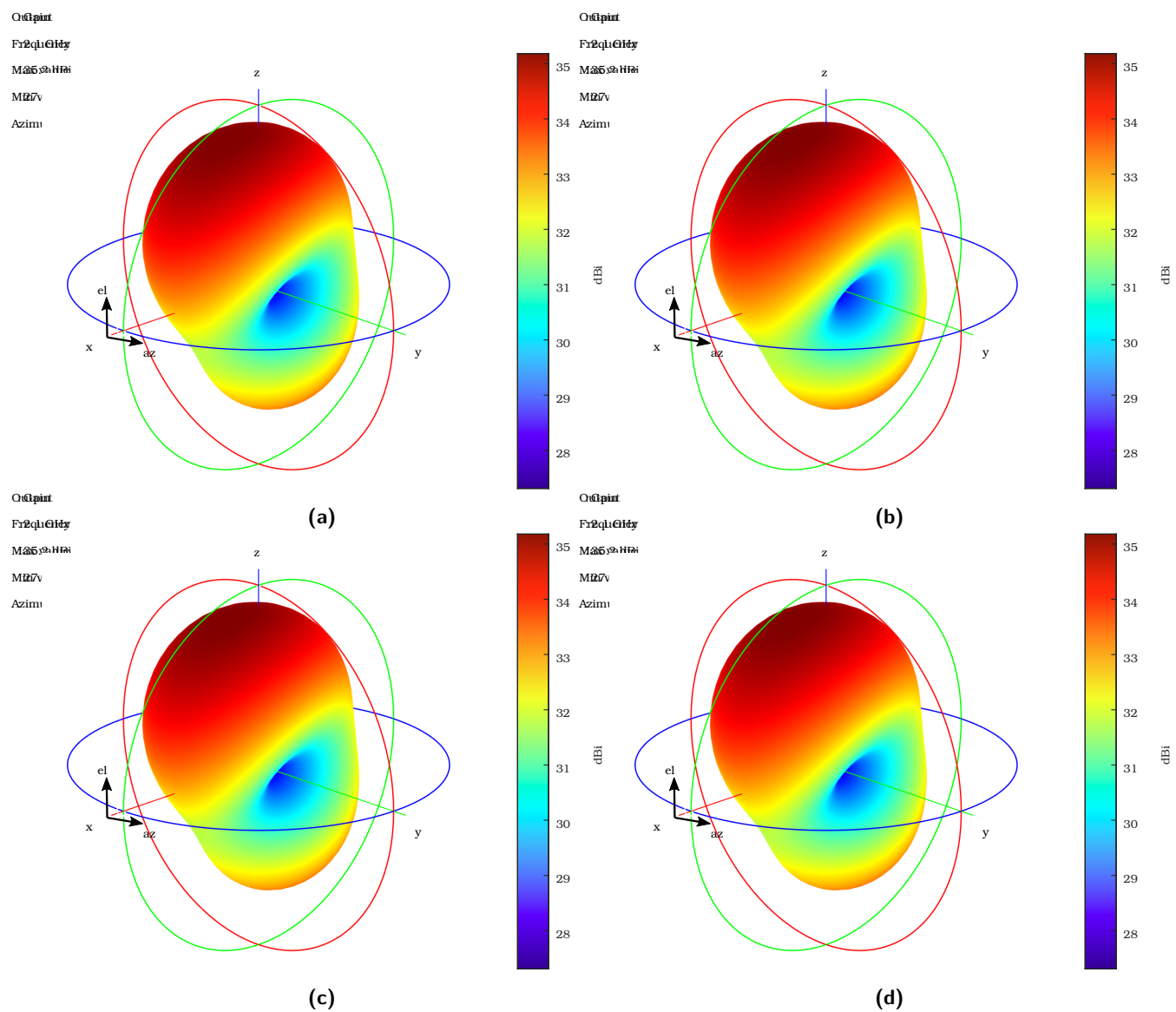


Figure 12: Gain pattern for PIFA (a) !!!! SOSTITUIRE QUESTI PATTERN CON GLI ALTRI !!!

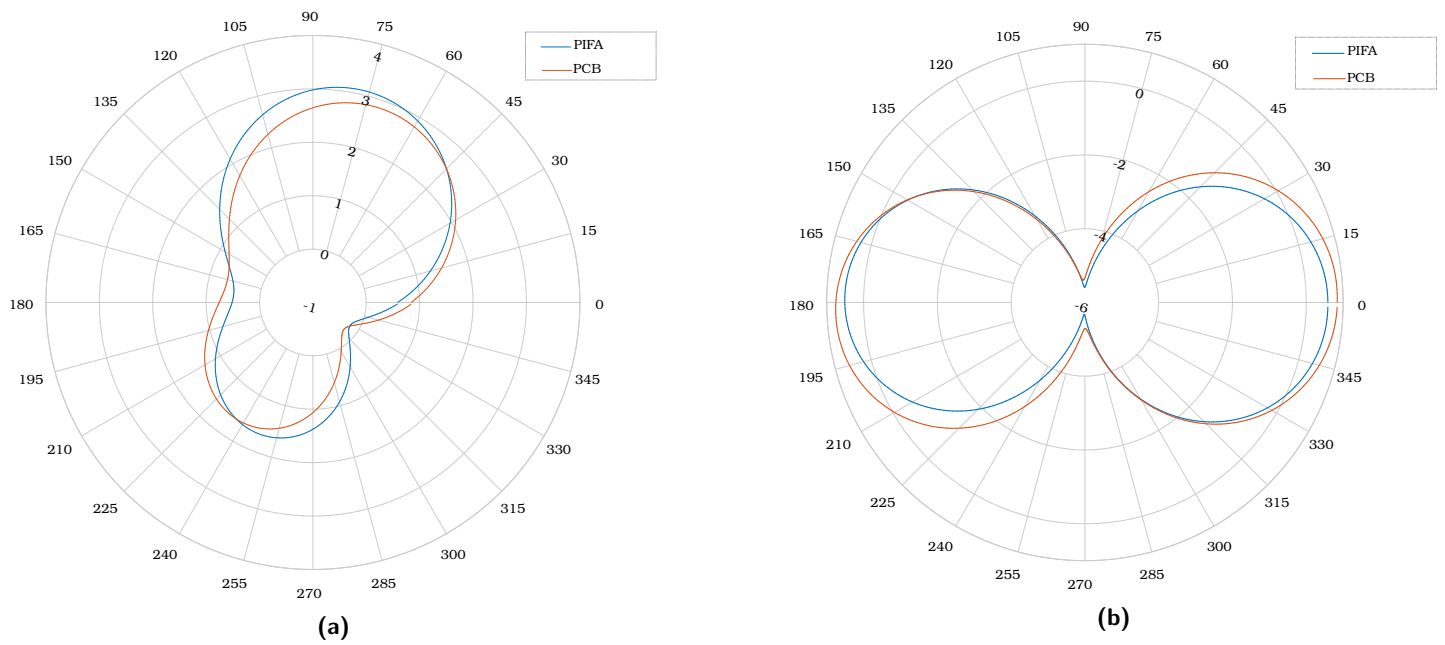


Figure 13: PIFA and PCB single antenna directivity patterns (dB) in the Azimuth cut ($\theta_{el} = 0^\circ$, (a)) and in the Elevation cut ($\phi_{az} = 0^\circ$, (b))

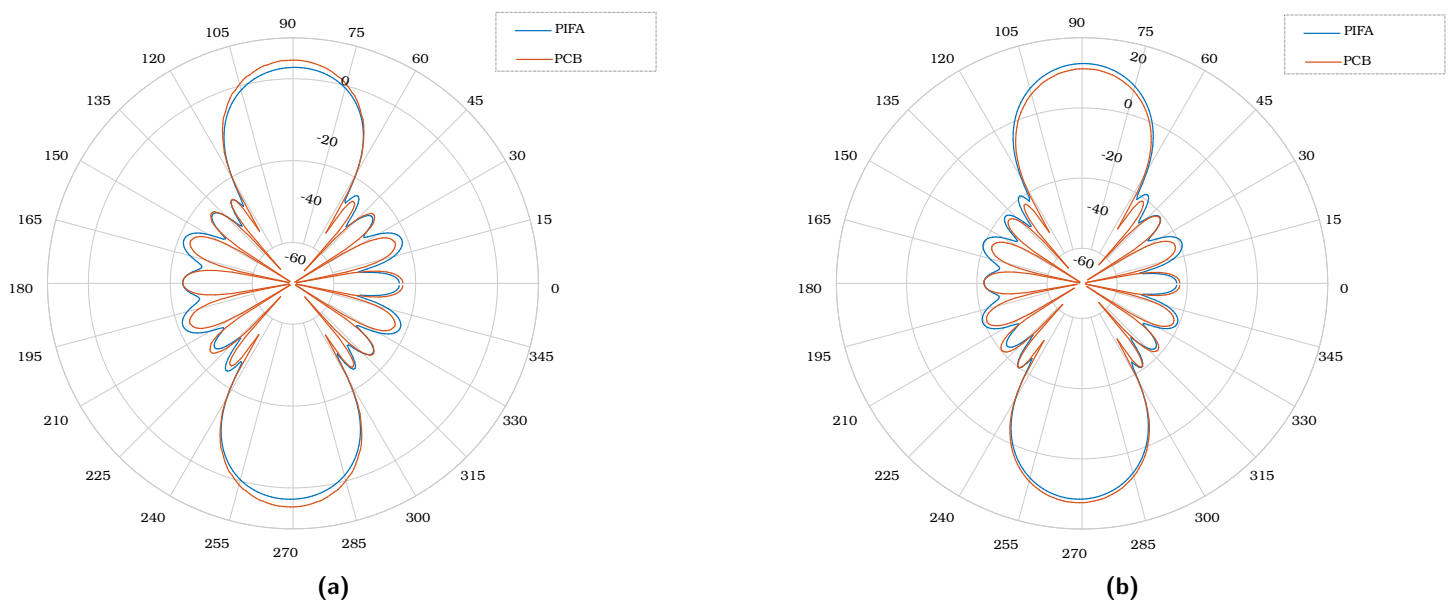
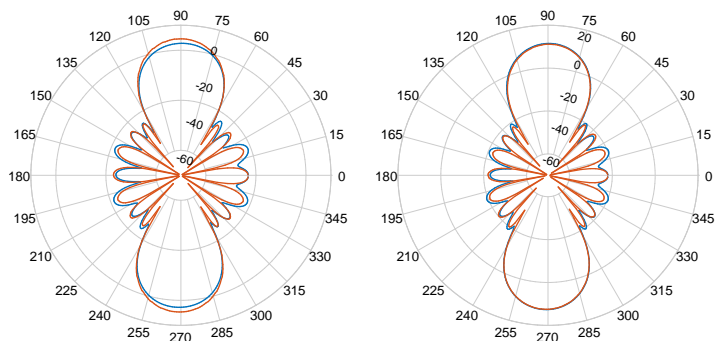
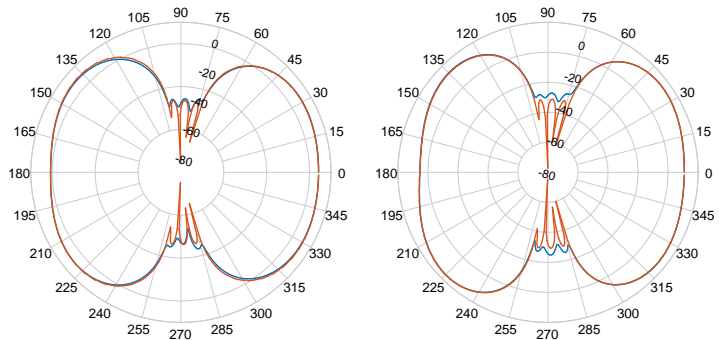


Figure 14: PIFA and PCB arrays directivity patterns (dB) in the Azimuth cut ($\theta_{el} = 0^\circ$, (a)) and in the Elevation cut ($\phi_{az} = 0^\circ$, (b))



(a)



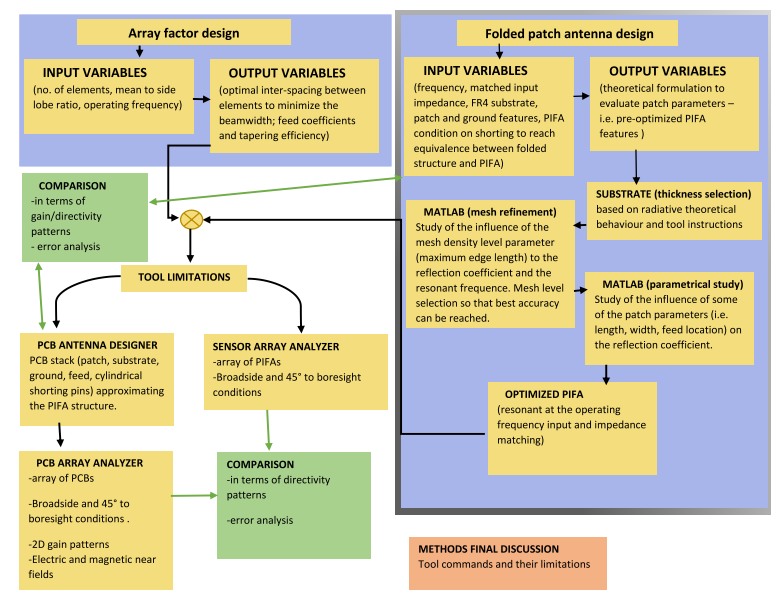
(b)

(c)

(d)

Figure 15: 2D patterns in both the broadside case ((a) azimuth cut and (b) elevation cut) and 45° off the boresight direction ((c) azimuth cut and (d) elevation cut).

Code



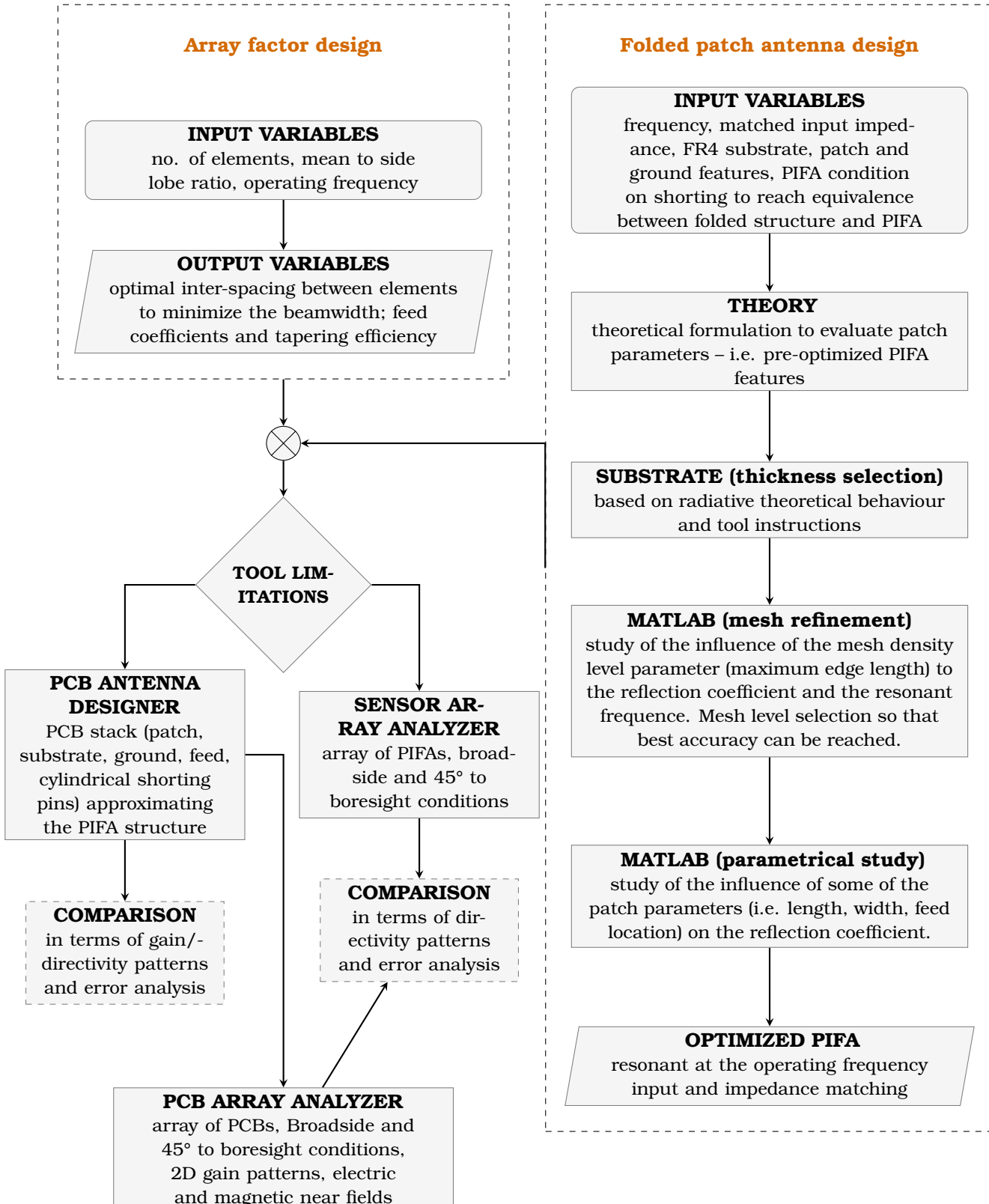


Figure 16

```

1 a=pattern();
2 a=pattern()
3 a=pattern()
4 mypath

```

Listing 1: Code